PHYSICAL CHEMISTRY
OF SOLUTIONS

Retention Behavior and Dynamic Sorption of Strontium Ions from Aqueous Media Using Fabricated Inorganic Sorbent

M. R. Abass[a], R. A. Abou-Lilah[a], and A. E. Kasem[a, *]

[a] *Egyptian Atomic Energy Authority, Hot Laboratories and Management Centre, Cairo, 13759 Egypt*
*e-mail: abeer_esmat@yahoo.com

Abstract—Sorption of Sr(II) from aqueous solutions has been studied using fabricated lithium magnesium boron silicate (LMBS) sorbent. LMBS sorbent has been fabricated by the co-precipitation technique and characterized using different analytical tools like ATR, SEM, TGA, DTA, and XRD. The sorption studies applied on Sr(II) include the effect of shaking time, ionic strength, pH, and temperature. The sorption of Sr(II) is dependent on pH and ionic strength. Reaction kinetics follows the pseudo-2nd-order model, and thermodynamics are endothermic and spontaneous. The saturation capacity of sorbent calcined at temperatures 50, 200, 400, and 600°C has been found to be 144.1, 134.5, 130.3, and 113.0 mg g^{-1}, respectively. Desorption studies have revealed that HCl is the optimum eluent for full recovery of Sr(II) ions (about 96.8%). Finally, according to column data, Sr(II) can be loaded and recovered from aqueous solutions using different concentrations of HCl eluent. The investigation has proved that LMBS is a suitable sorbent material for the recovery of Sr(II) from liquid waste.

1. INTRODUCTION

Since the Fukushima nuclear accident in 2011, large amounts of radioactive nuclides have been released into the environment [1]. The released radioactive nuclides were deposited on the soil, houses, trees, plants, water, and other structures [2, 3]. The development and use of nuclear energy are accompanied by the generation of significant amounts of radioactive waste that cannot be ignored [4]. Radioactive strontium (^{90}Sr) is one of the most dangerous fission products because of its high fission yield (4.5%), medium half-life (28.9 years), emission of high-energy beta rays, and high solubility in water [5]. In addition, ^{90}Sr quickly accumulates in human bones through the food chain as it resembles calcium; causing blood and bone cancers [6]. To guarantee that the presence of ^{90}Sr in drinking water does not exceed the Environmental Protection Agency's upper radioactivity level of 0.3 Bq L^{-1}, which is equivalent to about 0.057 ppq (parts per quadrillion), therefor is very important to remove low concentrations of ^{90}Sr from natural water which contains a high level of competing species (Mg^{2+} and Ca^{2+}) [7]. Moreover, the presence of higher quantities of metals in the water/soil leads to severe diseases and can irreversibly endanger environmental ecosystems [8].

Therefore, for nuclear safety and avoidance of environmental pollution, specific and efficient treatments for strontium in the aquatic environment must be developed [9]. A different techniques have been used to remove ^{90}Sr from contaminated water, such as adsorption [10, 11], chemical precipitation [12], solvent extraction [13], membrane processes [14], and ion exchange [15], etc. Adsorption is regarded as the most promising technique for radioactive wastewater treatment as it can reduce large volumes of waste into a more stable solid form considering its ease of use, affordability, effectiveness, and high capacity.

Therefore, the development of different stable adsorbents is essential for ^{90}Sr decontamination, particularly those inorganic ones with high selectivity, high adsorption affinity, and high thermal, chemical, and radiation resistance [16]. Strontium has been removed from aquatic environments using various kinds of organic and inorganic adsorbents, such as natural zeolites, porous carbon composites, graphene oxides, ammonium molybdophosphate composites, hydroxyapatites, and sodium titanates [9, 17, 18].

Composite ion exchangers based on silica are regarded as the most effective ones for the selective removal of heavy metals from wastewater [19–21]. The impregnation of different metal ions inside silica layers to prepare effective sorbent materials such as MgSi [22], SiSb [23], and ZrSiSb [24], was previously carried out. Still, the impregnation of Li, Ba, and Mg inside silica layers has not been carried out yet to

Table 1. Conditions for the synthesis of different sorbents and their % S.E. of Sr(II) at 200 mg L^{-1}, V/m = 100 mL g^{-1}, shaking time 24 h, and at room temperatures

Solutions and % S.E.	Samples			
	S-1 (MCBS)	S-2 (MCAS)	S-3 (LMBS)	S-4 (LMBSC)
LiCl, [0.5 M]	0 mL	0 mL	100 mL	100 mL
MgCl$_2$·6H$_2$O, [0.5 M]	250 mL	250 mL	100 mL	100 mL
CdCl$_2$·2.5H$_2$O, [0.5 M]	250 mL	250 mL	0 mL	0 mL
AlCl$_3$·6H$_2$O, [0.5 M]	0 mL	250 mL	0 mL	0 mL
H$_3$BO$_3$ [0.5 M]	250 mL	0 mL	100 mL	100 mL
Na$_2$SiO$_3$·9H$_2$O, 10% (W/V)	250 mL	250 mL	100 mL	100 mL
CMC, 4% (W/V)	0 mL	0 mL	0 mL	400 mL
% S.E.	32.8	22.5	98.5	75.6

obtain a lithium magnesium boron silicate (LMBS) as a novel sorbent material with high sorption efficiency to Sr(II) from aqueous solutions. In this paper, the sorption behavior of Sr(II) from aqueous solutions onto prepared LMBS sorbent was studied. Characterization of the synthesized sorbent has been done by using different tools. Under various batch experimental conditions, LMBS sorbent was applied for the separation of Sr(II) from their aqueous solutions.

2. EXPERIMENTAL

2.1. Material. The reagents utilized in this study were all analytical grades and weren't cleaned additionally. For all of the studies, double-distilled water (DDW) was utilized. Lithium chloride (LiCl), boric acid (H$_3$BO$_3$), magnesium chloride hexahydrate (MgCl$_2$·6H$_2$O), cadmium chloride hemi(pentahydrate) (CdCl$_2$·2.5H$_2$O), sodium metasilicate nonahydrate (Na$_2$SiO$_3$·9H$_2$O), and carboxymethylcellulose (CMC) with high viscosity (400−800 cps) (Loba Chemie, India). Strontium chloride (SrCl$_2$), aluminum chloride hexahydrate (AlCl$_3$·6H$_2$O), and hydrochloric acid (HCl) (Merck, Germany). Sodium chloride (NaCl) and sodium hydroxide (NaOH) (El-Nasr Co, Egypt).

2.2. Preparation. Different sorbent materials were prepared using co-precipitation method by dropwise of equimolar solutions (0.5 M) of LiCl, MgCl$_2$·6H$_2$O, H$_3$BO$_3$, CdCl$_2$·2.5H$_2$O, and AlCl$_3$·6H$_2$O to 10% (W/V) Na$_2$SiO$_3$·9H$_2$O and 4% (W/V) CMC solutions by different volumetric ratios as shown in Table 1, with constant stirring for 2 h. Drops of concentrated HCl were added to mixture solutions and a white gel was produced at pH (8.0), and the synthesized mixture was left without stirring overnight, then washed with DDW, and dried at 60 ± 1°C. After that the dried solid was converted into H$^+$ form by mixing it with 0.1 M HNO$_3$ for 24 h, it was then filtered and washed several times with DDW to get rid of excess HNO$_3$, finally, it was dried at 60 ± 1°C.

2.3. Instruments for sorbent and sorbate characterization. LMBS sorbent was analyzed with X-ray diffraction (XRD) and attenuated total reflectance (ATR) spectrum using Brucker XRD diffractometer D2 Phaser II, Germany, and Alpha II Bruker, Germany, respectively. Approximately 30 mg of LMBS sorbent per sample was used to analyze the morphologies under a scanning electron microscope (SEM) (JSM-6510A Model, Japan). A Shimadzu DTG-60 H was used to perform thermogravimetric (TGA) and differential thermal analysis (DTA) on LMBS sorbent. Using alumina powder as reference material (20 mg) samples were tested from the ambient temperature up to 800°C with a heating rate of 10 deg/min in N$_2$ atmosphere. The concentration of Sr(II) was determined using an atomic absorption spectrophotometer (AAS) (model S series, thermos electron copration, England).

2.4. Sorbents choice. For choosing the best sorbents of the differently prepared samples, a batch experiment was carried out by mixing 0.05 g of all prepared samples with 5 mL of Sr(II) at 200 mg L^{-1} with V/m = 100 mL g^{-1} in a shaker thermostat (Kottermann D-1362, Germany) at 298 ± 1 K. After 24 h, the solution is separated at once from the solid. Hence, the concentration of the tested ions was determined using AAS. Equation (1) can be used to compute the % sorption efficiency (S.E.) [25];

$$\% \, S.E. = \left(\frac{C_0 - C_f}{C_0} \right) \times 100, \qquad (1)$$

where C_0 and C_f are the initial and final concentrations of Sr(II) in solution respectively, and the data are tabulated in Table 1. These data exhibit that four sorbent materials: magnesium cadmium boron silicate (MCBS), magnesium cadmium aluminum silicate (MCAS), lithium magnesium boron silicate (LMBS), and lithium magnesium boron silicate @CMC (LMBSC) were prepared by the co-precipitation method. A great improvement in the % S.E. of Sr(II) LMBS sorbent, therefore LMBS sorbent was chosen

for all experimental tests. Also, the data presented in Table 1 indicated that the % S.E. of Sr(II) onto differently prepared samples has sequence; LMBS > LMBSC > MCBS > MCAS, these results prove that an improvement carried out to the LMBS sorbent by adding of lithium, while cadmium, aluminum, and CMC may be caused blocking to active sites.

2.5. Point of zero charges (PZC). To determine the point of zero charges (PZC) for LMBS sorbent, different samples (10 mL each) from 0.1 M NaCl were prepared in the pH range (1−12) using 0.1 M HCl and/or NaOH, then 0.1 g of the LMBS sorbent was stirred with each sample for 24 h at room temperature. The solutions were filtered and the pH of the filtrates was measured (pH final). The difference between initial pH_i and final pH_f ($\Delta pH = pH_f - pH_i$) was plotted against pH_i. The point of intersection at which ΔpH 0 is called pH_{Pzc}.

2.6. pH titration. The investigation of pH titration for LMBS sorbent was achieved by using the NaOH-NaCl system according to Topp and Pepper method [26]. 0.1 g of LMBS sorbent was shaken with each of the various 10 mL NaOH−NaCl systems. The pH of the solution was measured by a lab pH meter after one day until reached equilibrium.

2.7. Chemical stability. Different solvents were used to study the chemical stability of the LMBS sorbent such as alkaline, mineral acids, and some organic solvents, by shaking 0.2 g of solid with 20 mL of different solvents for about 3 days at $25 \pm 1°C$. The amount of LMBS sorbent released into the solution was determined gravimetrically [22].

2.8. Sorption studies. Several factors, such as pH (1−6), temperatures (25−65°C), and shaking time (2−60 min) are examined to obtain the optimum sorption conditions. The sorbent and the sorbate solution were contacted in a batchwise way and after sorption, the samples were separated from the solution by filtration. All equilibrium measurements were performed by shaking 0.05 g of LMBS sorbent with 5 mL of Sr(II) of the initial concentration of 200 mg L^{-1} with $V/m = 100$ mL g^{-1} in a shaker thermostat (Kottermann D-1362, Germany). In this investigation, all the tests were duplicated twice to ensure the validity of experimental data. The capacities at any time t (q_t, mg g^{-1}) and equilibrium (q_e, mg g^{-1}) of Sr(II) retained on the LMBS sorbent were determined utilizing the next equations, respectively [25, 27]:

$$q_t = (C_0 - C_t)\frac{V}{m}, \qquad (2)$$

$$q_e = (C_0 - C_e)\frac{V}{m}, \qquad (3)$$

where C_e and C_t are the equilibrium concentration and concentration at any time t of Sr(II) in the aqueous solution (mg L^{-1}); respectively; V is the volume of the solution (L), and m is the mass of the dried adsorbent (g).

2.9. Saturation capacity and thermal stability. Repeated batch equilibration of 200 mg L^{-1} Sr(II) was shaken with LMBS calcined at a different temperature ranging from (50−600°C), in $V/m = 100$ mL g^{-1}, temperature 25°C, it was then performed until no further sorption of Sr(II) for capacity measurement. The value of q_e was computed from Eq. (3). The saturation capacity of the LMBS sorbent could be determined by Eq. (4), using the total number of times added new volumes (n).

$$\text{Saturation capacity} = \sum_{e=1}^{n} q_e. \qquad (4)$$

2.10. The distribution coefficients. The distribution coefficients (K_d) as a function of pH were obtained from Eq. (5) [28, 29]:

$$K_d = \left(\frac{C_0 - C_f}{C_f}\right)\frac{V}{m} \quad \text{(mL/g)}. \qquad (5)$$

In this equation, V is the solution volume (mL).

2.11. Desorption studies. Desorption of Sr(II) loaded onto LMBS sorbent was investigated by a batch method at a fixed temperature of $25 \pm 1°C$, using many eluenting agents with a volume-to-sorbent ratio of 100 mL g^{-1}. The used eluents are 0.1 M of (HCl, NaCl, MgCl$_2$, CaCl$_2$, BaCl$_2$, EDTA, and AlCl$_3$). Loaded LMBS sorbent (0.05 g) was mixed with 5 mL of these eluents for 24 h, then the two phases were separated and the concentration of Sr(II) was detected in the solid phase (C_d) and the supernatant (C_s), mg L^{-1}. The % of desorption was computed using Eq. (6) [30]:

$$\% \text{ Desorption} = \left(\frac{C_s}{C_d}\right) \times 100. \qquad (6)$$

2.12. Column applications. Applications of chromatographic column were assumed as follows, 0.5 g of LMBS sorbent was put in a glass column. 500 mL of Sr(II) with an initial concentration of 200 mg L^{-1} at optimum pH 5 was passed through LMBS sorbent at a flow rate of 0.25 mL min^{-1}, all bottles were collected and the concentrations were measured. The values of breakthrough capacity (BTC, mg g^{-1}) were computed by the formula [31, 32];

$$\text{BTC} = V_{50\%}\frac{C_0}{m}, \qquad (7)$$

where $V_{50\%}$ and m are the effluent volume at 50% breakthrough (L) and the quantity of the column bed per gram, respectively.

DDW and various HCl concentrations (0.01, 0.05, 0.1, 0.25, and 0.5 M) were utilized to release the sorbed Sr(II) from the columns of LMBS at the same flow rate of column applications (0.25 mL min^{-1}).
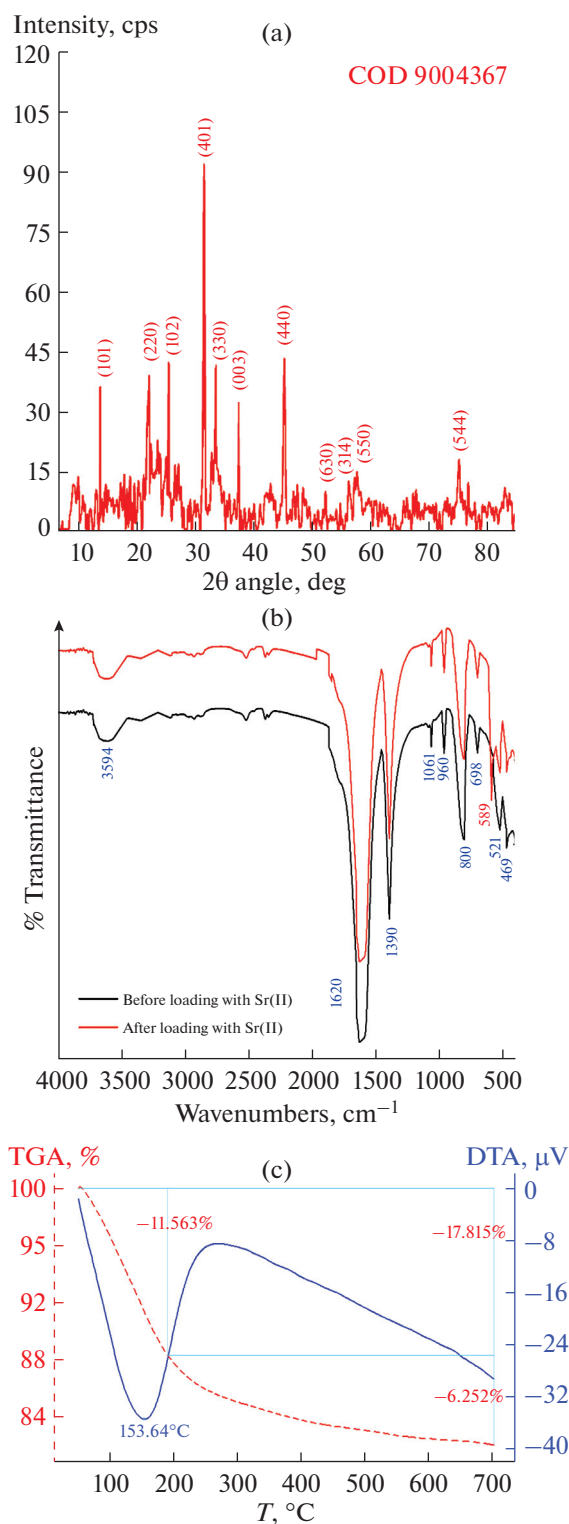
Fig. 1. (a) XRD analysis, (b) ATR spectrum before and after loading with Sr(II), and (c) TGA and DTA analysis of LMBS sorbent.

3. RESULTS AND DISCUSSION

3.1. XRD Analysis

The crystalline nature of LMBS sorbent was examined using X-ray diffraction (XRD) as shown in Fig. 1a. It was found that from this figure LMBS sorbent possesses a crystalline nature and shows many sharp peaks centered at 13.89°, 22.26°, 25.63°, 31.69°, 33.66°, 37.57°, 45.42°, 52.51°, 56.6°, 57.72°, and 75.39° related to Miller index indications 101, 220, 102, 401, 330, 003, 440, 630, 314, 550, and 544, respectively, with COD 9004367, with a matching of pure uvite that has a chemical formula $[Al_{5.916}B_3Ca_{0.716}Cr_{0.021}F_{0.915}$-$H_{6.085}Li_{0.057}Mg_{3.186}Na_{0.255}O_{33.085}Si_{5.586}Ti_{0.033}V_{0.201}]$ prepared by MacDonald et al. [33], confirming their crystalline nature with the hexagonal system.

3.2. ATR analysis

The ATR analysis of LMBS before and after sorption of Sr(II) was signified in Fig. 1b. Indeed, the corresponding infrared spectrum shows an absorption band at 3594 cm^{-1} attributed to the OH stretching mode (ν(OH)) of lithium hydroxide [34]. The peak at 1620 cm^{-1} was due to the H−OH bending vibrations of the adsorbed water molecules [35]. A broad band at 1389 cm^{-1} due to the stretching vibration of [B−O] bonds in the triangle and metaborate groups [36]. The band appearing at 960 cm^{-1} is due to the vibrations of bending modes of B−O−B links in the network of borate [37]. Four bands were noticed at 469 cm^{-1} (Si−O out-of-plane deformation), 800 cm^{-1} (Si−O bending), 960 cm^{-1} (Si−OH stretching), and 1061 cm^{-1} (Si−O−Si asymmetric stretching) [38]. The band at 521 cm^{-1} due to Si−O−Mg (bending vibration) [39]. FT-IR analysis shows that the spectrum either of LMBS before or after loading of Sr(II) is approximately the same with a very slight shift except for the peak observed at 589 cm^{-1} which confirms the sorption of Sr(II) onto the surface of LMBS sorbent.

3.3. Thermal Analysis

Figure 1c represents thermogravimetric analyses (TGA) of LMBS sorbent heated at the rate of 10°C/min, via a two-stage process for LMBS sorbent. The first stage (49.6−190.4°C) is a result of the elimination of H_2O physically adsorbed onto the surface of the LMBS sorbent [22], and the weight loss in this region is (11.56%). In the second stage (190.4−701.1°C) as a result of the loss of chemically bonded H_2O [32], at this region there is a weight loss of about (6.25%). Differential thermal (DTA) shows one endothermic peak at (153.6°C) due to loss of free H_2O, This peak resembles the bentonite dolomite composite's thermal analysis synthesized by Abass et al. [40]. From the data of TGA in Fig. 1c, the weight loss for LMBS sorbent continued up to 700°C. The weight loss of

LMBS sorbent with the heating temperature that a (17.815%). This weight loss was obtained when the sample was calcinated at 700°C.

3.4. Surface Morphology

SEM pictures of LMBS were represented in Fig. 2 at many magnification powers (×500, ×1000, and ×2000). The pictures show a non-homogeneous distribution of the lithium, magnesium, and boron particles (white) on the silica sheets (grey). At magnification power of ×500, the surface of LMBS appears to have very small porous, by increasing the magnification power at ×1000 and ×2000, the particles were rugged, sharp, and possess intermolecular distances that support the physical sorption of Sr(II) on LMBS.

3.5. Point of Zero Charges (PZC) Detection, Sr(II) Speciation, and pH Titration

PZC for LMBS sorbent provides us with more information about the ionization of functional groups and their interaction with Sr(II). Plots of ΔpH vs pH_i as represented in Fig. 3a to determine PZC for LMBS sorbent, the value of ΔpH increased with increasing pH_i then reduced and PZC was determined at pH 3.73. These data agreed with the sorption of Sr(II) onto LMBS sorbent as seen later.

The speciation of Sr(II) was achieved by the MEDUSA program at a pH range (1−12) and ionic strength of 0.001 as illustrated in Fig. 3b. The data showed that the speciation of Sr(II) has no precipitate at pHs (1−12) [41]. The concentration of H^+ ions was reduced with increasing pH values and at pH value 9, H^+ ions disappeared as well, and at pH 5, OH^- ions started to increase with the formation of species $(SrOH^+)$ at pH 9.3.

Figure 3c shows the pH titration of LMBS sorbent. The *X*-axis characterizes the number of millimoles of 0.1 M NaOH passed through per gram of LMBS sorbent and the *Y*-axis shows the pH of the effluent. The data show only one inflection point indicating that the LMBS sorbent has one function group for the sorption of Sr(II). This behavior is similar to cerium(IV) molybdate [42] and SnSiMo [43].

3.6. Chemical Stability

The chemical stability test for LMBS sorbent toward different reagents (Table 2) reflected that the prepared sorbent was very stable in many organic solvents, alkalis, and common mineral acids. Table 2 shows that LMBS sorbent has relatively high stability to chemicals compared to other sorbents [25].
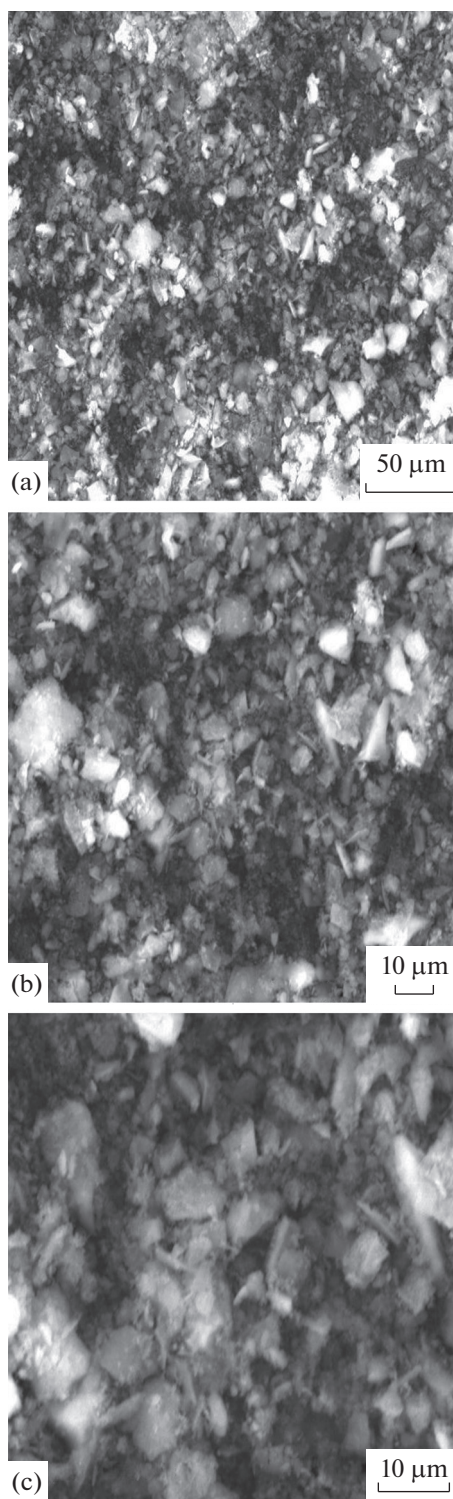

Fig. 2. SEM images of LMBS sorbent at different magnification powers (a) ×500, (b) ×1000, (c) ×2000.

3.7. Influence of pH

The sorption efficiency (% S.E.) of Sr(II) on the synthesized LMBS sorbent from aqueous solutions was investigated as seen in Fig. 4a. As seen in this
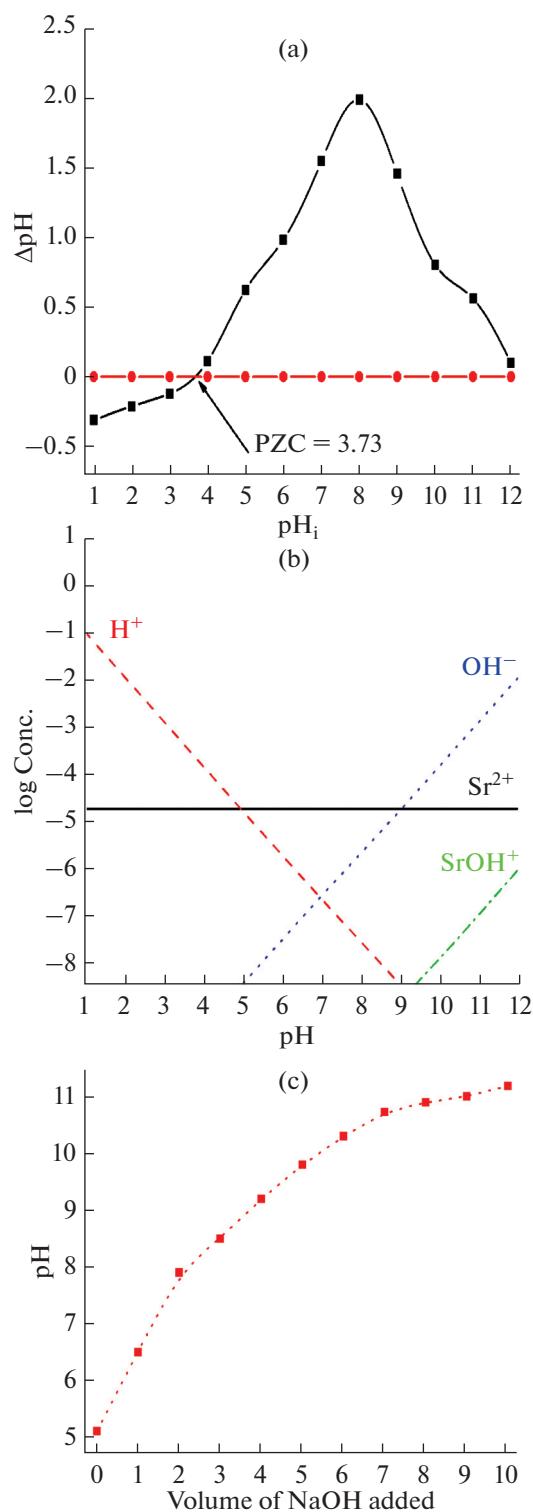
Fig. 3. (a) Plots of ΔpH vs pH$_i$ for PZC, (b) speciation at room temperature and 0.001 ionic strength, and (c) pH titration curve for LMBS sorbent.
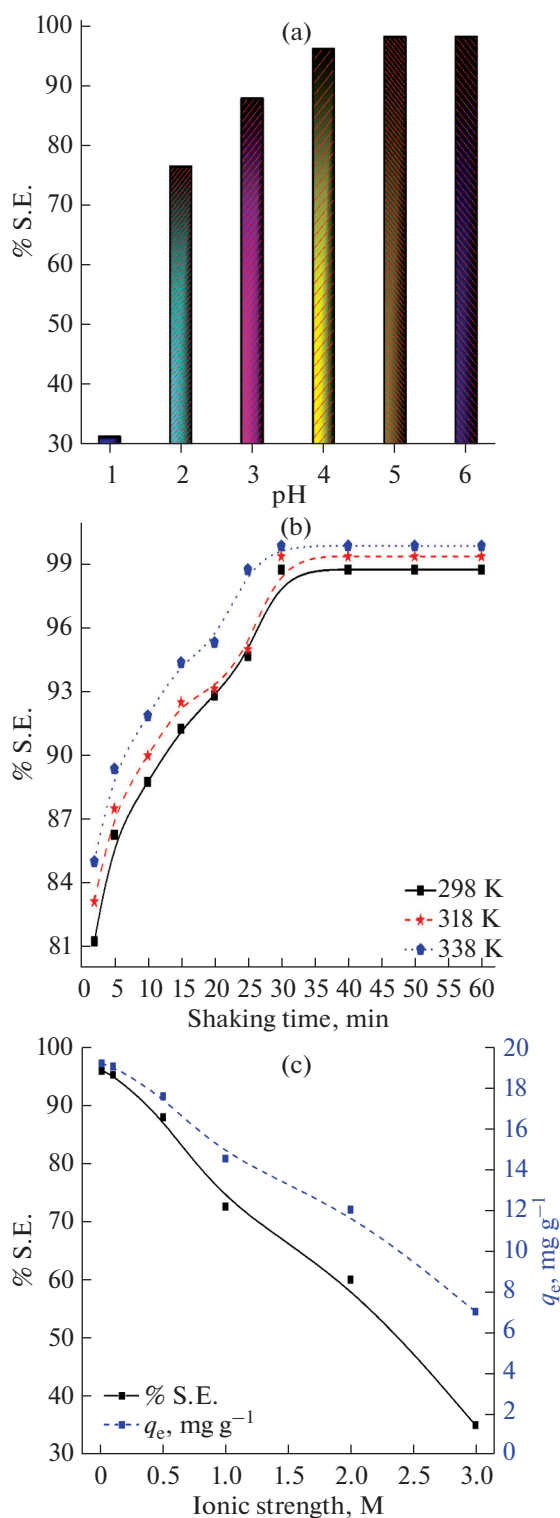

Fig. 4. Sorption of Sr(II) onto LMBS sorbent: (a) effect of pH on the % S.E., (b) effect of shaking time on the % S.E., and (c) effect of ionic strength on the % S.E. and amount uptake.

Fig. 4, there was an increase in the % S.E. with increasing pH (1−5) from 31.7 to 98.7%. Above this pH value, no change was observed for the % S.E and

all experimental work was performed at pH 5. Furthermore, it was found that at small pH values, the % S.E. of Sr(II) is small which is due to the protonation of the

Table 2. Chemical stability of LMBS sorbent in different solvents

Solvents	% Solubility
DDW	Below detection limit
Ethanol	1.1
Methyl ethyl ketone	2.15
0.5 mol/L HNO$_3$	0.99
3 mol/L HNO$_3$	5.55
0.5 mol/L HCl	2.1
3 mol/L HCl	6.28
0.5 mol/L KOH	3.5
1 mol/L KOH	18.6

surface of LMBS sorbent and the increase of H_3O^+ ions in the aqueous solutions. As a result of the positively charged surface sites, H_3O^+ and Sr(II) competed for the available binding surface active site, resulting in decreased Sr(II) sorption. As the initial pH value increased, the concentration of H_3O^+ ions decreased while the concentration of OH^- ions increased, causing sorbent surface deprotonation; such results indicate that the surface of the LMBS sorbent has a negative charge. Which enhances the attraction between the sorbent's surface and the positively charged Sr(II) in the solution. These data are compatible with the PZC of LMBS sorbent (3.73).

3.8. Effect of Shaking Time

The influence of shaking time on % S.E. of Sr(II) on the synthesized LMBS was performed at different temperatures (298−338 K), $C_0 = 200$ mg L^{-1}, $V/m = 100$ mL g^{-1}, shaking time (5−60 min), and pH 5, the obtained data are given in Fig. 4b. The % S.E. of Sr(II) on the synthesized LMBS sorbent increases with time and attained equilibrium at ~30 min. There is a rapid increase in the rate of Sr(II) uptake onto LMBS sorbent with time from 5 to 25 min, a slow increase in time was observed from 25 to 30 min, and the uptake hasn't changed above this time, for additional experimental work, 30 min used to be the equilibrium time. In addition, the data show that the % S.E. of Sr(II) on the synthesized LMBS sorbent increases with temperature reflecting the endothermic nature of the

sorption process. The increase in adsorption with increasing temperatures up to 65°C is due to increased penetration of Sr(II) inside pores at higher temperatures or the creation of new active sites [44].

3.9. Influence of Ionic Strength

The plots between the % S.E. and amount uptake (q_e, mg g^{-1}) of Sr(II) onto LMBS sorbent and the ionic strength of NaCl (0.01−3 M) are shown in Fig. 4c. The experiment was performed at [$C_0 = 200$ mg L^{-1}, $V/m = 100$ mL g^{-1}, shaking time 30 min, and pH 5]. Figure 4c exhibits a great decrease in the % S.E. and q_e of Sr(II) with rising ionic strength leading to ionic strength dependence, the strong ionic strength dependence is mainly dominated by β-plane sorption [45].

3.10. Thermal Stability and Saturation Capacity

The saturation capacity of LMBS sorbent that was calcined at temperatures (50, 200, 400, and 600°C) toward Sr(II) was determined at 25 ± 1°C and the results are summarized in Table 3. A significant decrease in capacity was seen with increasing calcining temperatures, which corresponded to the degradation of the water content in TGA&DTA data [46]. LMBS sorbent has a good retention behavior up to 600°C, and this behavior reflects its thermal stability. Also, the data on the saturation capacity of LMBS calcined at different temperatures are higher than that reported by Abass et al. [35].

3.11. Kinetic Study

Pseudo-1st-order and pseudo-2nd-order were utilized to investigate and analyze the computed data from the sorption of Sr(II) onto LMBS sorbent at different reaction temperatures and can be calculated from Eqs. (7) and (8) [47]:

$$\log(q_e - q_t) = \log q_e - \frac{K_f t}{2.303}, \qquad (7)$$

$$\frac{t}{q_t} = \frac{1}{K_s q_e^2} + \frac{t}{q_e}, \qquad (8)$$

in which, K_f (min^{-1}) and K_s (g mg^{-1} min^{-1}) are the rate constants of two kinetic models. Plotting $\log(q_e - q_t)$ and t/q_t against t for pseudo-1st-order and pseudo-

Table 3. Effect of calcining temperatures of LMBS sorbent on the saturation capacity of Sr(II)

Calcining temperature, °C	Weight loss, %	Saturation capacity, mg g^{-1}	% Retention
50	Nil	144.1	100.0
200	3.35	134.5	93.3
400	12.1	130.3	90.4
600	16.1	113.0	78.4

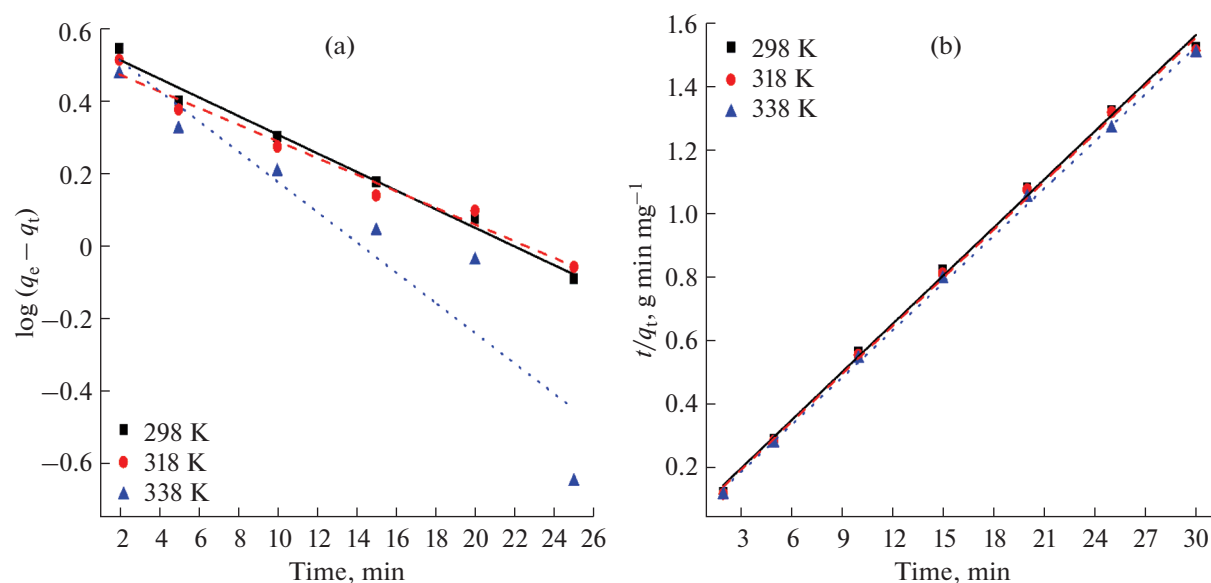**Fig. 5.** Kinetic modeling fitting of Sr(II) onto LMBS sorbent at different reaction temperatures [$C_0 = 200$ mg L^{-1}, $V/m = 100$ mL g^{-1}, and pH = 5], (a) pseudo-1st-order kinetic and (b) pseudo-2nd-order kinetic.

2nd-order linear relations, respectively as shown in Fig. 5. The plot of pseudo-1st-order relations displays straight lines with a bad linearity while the pseudo-2nd-order plot illustrates straight lines with a good linearity. K_f, K_s, and R^2 computed from these plots were tabulated in Table 4. These data reveal that pseudo-2nd-order kinetic is the major mechanism, as R^2 for Sr(II) is high and closer to unity and more than the pseudo-first-order model as well as the values of q$_e$ (cal.) for pseudo-2nd-order very close to q_e (exp.). This means the adsorption of Sr(II) onto LMBS sorbent is controlled by a chemisorption process [48].

3.12. Thermodynamic Studies

The linear relation between $\ln K_d$ of Sr(II) onto LMBS and $1000/T$ were shown in Fig. 6a based on Van't Hoff relation [49]:

$$\ln K_d = \frac{\Delta S^\circ}{R} - \frac{\Delta H^\circ}{RT}, \qquad (9)$$

where ΔS°, ΔH°, R, and T are the entropy change of adsorption, enthalpy change of adsorption, gas con-

stant, and absolute temperature, respectively. As represented in Fig. 6a, K_d of Sr(II) improved with rising temperature from (298−338 K). This enhancement of the adsorption process is related to the acceleration of previously slow adsorption steps and the formation of new active sites on the surface of LMBS [50]. From both slopes and intercepts of the straight lines exhibited in Fig. 6, ΔH° and ΔS° were computed and represented in Table 5. The positive values of ΔH° reflect the endothermic nature of the adsorption process [50]. The positive values of ΔS° indicate the increased randomness of the solid solution interface during the adsorption of Sr(II) onto LMBS sorbent [50]. The data in Table 5 reveal that the value of ΔH° for Sr(II) onto LMBS sorbent is 47.56 kJ mol^{-1} at pH 5 which indicates the presence of another mechanism for the adsorption of Sr(II) onto LMBS sorbent beside the ion exchange mechanism [51]. The free energy change of specific adsorption (ΔG°) was calculated using equation (10):

$$\Delta G^\circ = \Delta H^\circ - T\Delta S^\circ. \qquad (10)$$

The negative values of ΔG° presented in Table 5 reveal that the adsorption process is spontaneous and

Table 4. Kinetic parameters and correlation coefficients (R^2) for pseudo-1st-order, and pseudo-2nd-order models for the sorption of Sr(II) onto LMBS sorbent at different reaction temperatures

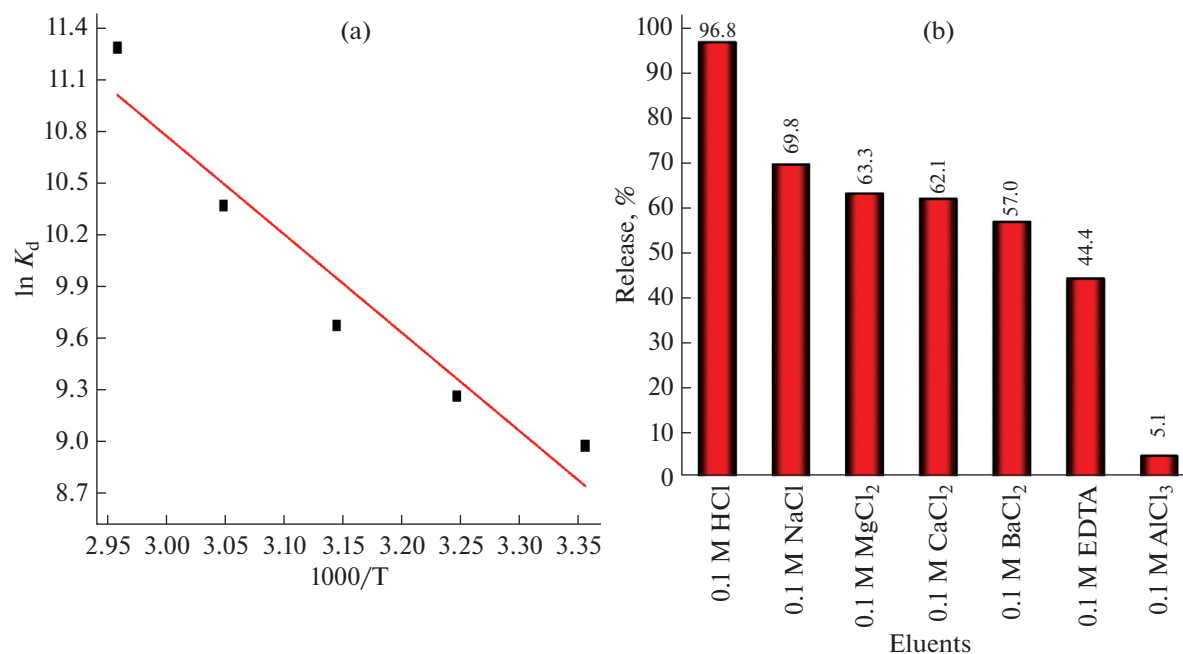| Reaction temperature, K	q_e (exp.)	Pseudo-1st-order			Pseudo-2nd-order		
		q_e (cal.)	K_f	R^2	q_e (cal.)	K_s	R^2
298	19.75	3.66	0.059	0.985	19.85	0.055	0.997
318	19.88	3.29	0.053	0.969	19.89	0.061	0.997
338	19.98	3.93	0.096	0.852	20.23	0.064	0.999

Fig. 6. (a) A plot of $\ln K_d$ against 1000/T for sorption of Sr(II) onto LMBS sorbent [$C_0 = 200$ mg L^{-1}, $V/m = 100$ mL g^{-1}, and pH = 5] and (b) desorption of Sr(II) loaded onto LMBS sorbent using different eluents.

reflects the desirable adsorption of Sr(II) onto LMBS sorbent compared with the H$^+$ ion [52].

3.13. Desorption Studies

The desorption of Sr(II) loaded onto LMBS sorbent using many eluent agents was performed in a batch technique and the data were exposed in Fig. 6b. The data show that the Sr(II) is difficult to release from the surface of LMBS by rinsing with AlCl$_3$. While it is easily released by rinsing with NaCl, MgCl$_2$, CaCl$_2$, BaCl$_2$, and EDTA solutions. The great desorption of Sr(II) from the loaded on LMBS sorbent was performed using 0.1 M HCl as eluent. Hence, the efficiency of the used desorbing agents to release Sr(II) from the loaded LMBS follows the order: HCl (96.8%) > NaCl (69.8%) > MgCl$_2$ (63.3%) ≥ CaCl$_2$ (62.1%) > BaCl$_2$ (57.0%) > EDTA (44.4%) > AlCl$_3$ (5.1%).

3.14. Chromatographic Applications

The breakthrough curve for Sr(II) (200 mg L^{-1}) sorbed onto the LMBS column was represented in Fig. 7a. Figure 7a represents the plot of the percent concentrations of Sr(II) in the effluent to the feed solution (C/C_0 %) vs effluent volume, V (L). The BTC for the Sr(II) was calculated using Fig. 7a and using Eq. (7) and was found to be 134.2 mg g^{-1}. By comparison between the capacity performed by batch and column methods, the BTC is lower than that of the saturation capacity, this is related to the speed dynamic motion of Sr(II) through the column bed. Also, the BTC of present work is higher than the BTC of Sr(II) through the binary system (Pb–Sr) and multicomponent system (Pb–Cd–Co–Zn–Sr) using P(AA-AN)-talc nanocomposite [35].

The elution data for Sr(II) were examined in Fig. 7b using DDW and various HCl concentrations (0.01, 0.05, 0.1, 0.25, and 0.5 M). From Fig. 7b no release of

Table 5. Thermodynamic parameters for the sorption of Sr(II) onto LMBS sorbent

Temperature, K	$\Delta H°$, kJ mol^{-1}	$\Delta S°$, J mol^{-1} K^{-1}	$\Delta G°$, kJ mol^{-1}
298			−21.66
308			−23.98
318	47.56	232.3	−26.31
328			−28.63
338			−30.95

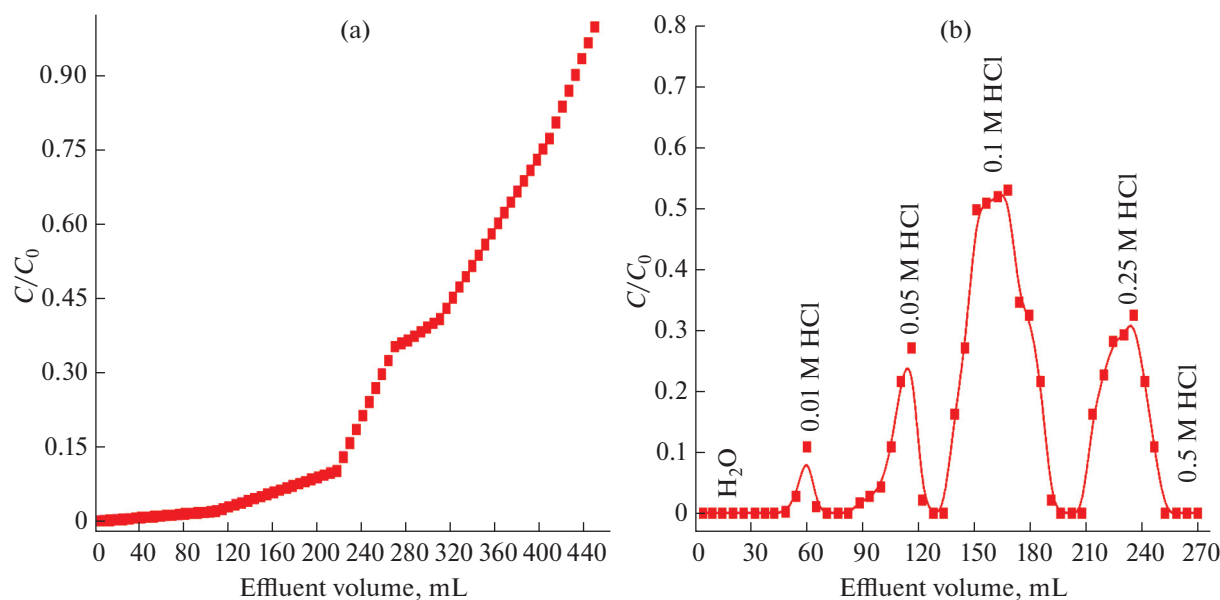**Fig. 7.** (a) Column operation for loading of Sr(II) sorbed onto LMBS sorbent at $25 \pm 1°C$ and (b) chromatographic elution of Sr(II) sorbed onto LMBS by H_2O and different concentrations of HCl at $25 \pm 1°C$.

Sr(II) by DDW. A slight release of Sr(II) was observed using (0.01 and 0.05 M) of HCl as eluents, while a great release of Sr(II) was observed using (0.1 and 0.5 M) of HCl as eluents. In addition, Fig. 7b reveals that at 0.5 M of HCl, the column packed with LMBS sorbent becomes free from any Sr(II). Therefore, LMBS sorbent it can be used for chromatographic applications as a best sorbent for the recovery of Sr(II) from liquid waste.

4. CONCLUSIONS

LMBS sorbent was fabricated by co-precipitation technique. LMBS was characterized and used for batch sorption of Sr(II) from aqueous media. The sorption data of Sr(II) confirms that LMBS has an equilibrium time of 30 min, applicable for pseudo-2nd-order kinetic, and thermodynamic parameters have spontaneous and endothermic. Solutions of HCl show optimum desorption of Sr(II). Finally, column application results prove that Sr(II) can be loaded and separated from an aqueous solution using various concentrations of HCl as a desorbing agent. The investigation supported that LMBS sorbent is suitable for the recovery of Sr(II) from liquid waste.

AUTHOR CONTRIBUTION

M.R. Abass: Conceptualization, Visualization, experimental work, writing-reviewing, and editing. R.A. Abou-Lilah: Experimental work, Data curation, writing—original draft review and editing. A.E. Kasem: Experimental work, Editing, and reviewing.

CONFLICT OF INTEREST

The authors declare that they have no conflicts of interest.

REFERENCES

1. Y. Shao, Y. Zhao, M. Luo, G. Zhao, D. Xu, Z. Liu, and L. Ma, Processes **11**, 379 (2023).

2. Y. Nishiyama, T. Hanafusa, J. Yamashita, Y. Yamamoto, and T. Ono, J. Radioanal. Nucl. Chem. **307**, 1279 (2016).

3. S. Mikami, T. Maeyama, Y. Hoshide, R. Sakamoto, S. Sato, N. Okuda, S. Demongeot, R. Gurriaran, Y. Uwamino, and H. Kato, J. Environ. Radioact. **139**, 320 (2015).

4. W.-A. Li, Y.-C. Peng, W. Ma, X.-Y. Huang, and M.-L. Feng, Chem. Eng. J. **442**, 136377 (2022).

5. D. Delacroix, J. P. Guerre, P. Leblanc, and C. Hickman, Radiat. Prot. Dosim. **98**, 1 (2002).

6. H.-M. Yang, H. Jeon, Y. Lee, and M. Choi, Chemosphere **299**, 134309 (2022).

7. J. Yang, W. Tai, F. Wu, K. Shi, T. Jia, Y. Su, T. Liu, P. Mocilac, X. Hou, and X. Chen, Chemosphere **292**, 133401 (2022).

8. S. A. Predoi, S. C. Ciobanu, M. C. Chifiriuc, M. Motelica-Heino, D. Predoi, and S. L. Iconaru, Materials **16**, 229 (2023).

9. G. Kim, D. S. Lee, H. Eccles, S. M. Kim, H. U. Cho, and J. M. Park, RSC Adv. **12**, 18936 (2022).

10. S. B. Yarusova, P. S. Gordienko, O. O. Shichalin, E. K. Papynov, E. A. Nekhliudova, A. V. Perfilev, S. Y. Budnitskiy, N. V. Zarubina, Y. A. Parotkina, and A. N. Drankov, Russ. J. Inorg. Chem. **67**, 1386 (2022).

11. E. A. Kutikhina, E. V Mazurova, O. V Buyko, T. A. Vereshchagina, and A. G. Anshits, Glass Phys. Chem. **49**, 167 (2023).

12. X. Luo, G. Zhang, X. Wang, and P. Gu, J. Radioanal. and Nucl. Chem. **298**, 931 (2013).

13. C. Xu, J. Wang, and J. Chen, Solv. Extract. Ion Exchange **30**, 623 (2012).

14. N. Rawat, P. K. Mohapatra, D. S. Lakshmi, A. Bhattacharyya, and V. K. Manchanda, J. Membr. Sci. **275**, 82 (2006).

15. M. Chandramouli, V. Basavanna, and S. Ningaiah, Russ. J. Gen. Chem. **93**, 1523 (2023).

16. Z. Jiao, Y. Meng, C. He, X. Yin, X. Wang, and Y. Wei, Microporous Mesoporous Mater. **318**, 111016 (2021).

17. E. S. Dragan and M. V. Dinu, React. Funct. Polym. **146**, 104372 (2020).

18. H. Zhang, C. S. Hodges, P. K. Mishra, J. Y. Yoon, T. N. Hunter, J. W. Lee, and D. Harbottle, ACS Appl. Mater. Interfaces **12**, 33173 (2020).

19. S. Nayab, A. Farrukh, Z. Oluz, E. Tuncel, S. R. Tariq, H. ur Rahman, K. Kirchhoff, H. Duran, and B. Yameen, ACS Appl. Mater. Interfaces **6**, 4408 (2014).

20. L. Chen, Y. Chen, X. Wang, Y. Wei, L. He, and F. Tang, J. Radioanal. Nucl. Chem. **314**, 2569 (2017).

21. E. S. Dragan, D. Humelnicu, M. Ignat, and C. D. Varganici, ACS Appl. Mater. Interfaces **12**, 44622 (2020).

22. M. R. Abass, H. M. Diab, and M. M. Abou-Mesalam, Silicon **14**, 2555 (2022).

23. M. R. Abass, M. A. Eid, and A. B. Ibrahim, Int. J. Environ. Anal. Chem. (2022). https://doi.org/10.1080/03067319.2022.2071611

24. M. R. Abass, W. M. El-Kenany, and M. A. Eid, Appl. Radiat. Isotopes **192**, 110542 (2023).

25. R. S. Hassan, M. R. Abass, M. A. Eid, and E. A. Abdel-Galil, Appl. Radiat. Isotopes **178**, 109985 (2021).

26. V. K. Gupta, G. Sharma, D. Pathania, and N. C. Kothiyal, J. Ind. Eng. Chem. **21**, 957 (2015).

27. M. M. Hamed, A. M. Shahr El-Din, and E. A. Abdel-Galil, J. Radioanal. Nucl. Chem. **322**, 663 (2019).

28. S. S. Metwally, H. S. Hassan, and N. M. Samy, J. Mol. Liq. **287**, 110941 (2019).

29. I. M. Ahmed, R. F. Aglan, and M. M. Hamed, J. Radioanal. Nucl. Chem. **314**, 2253 (2017).

30. G. A. Dakroury, E. A. A. El-Shazly, and H. S. Hassan, J. Radioanal. Nucl. Chem. **330**, 159 (2021).

31. M. R. Abass, E. H. El-Masry, and A. B. Ibrahim, Environ. Geochem. Health **43**, 3169 (2021).

32. M. M. Abou-Mesalam, M. R. Abass, E. S. Zakaria, and A. M. Hassan, Silicon **14**, 7961 (2022).

33. D. J. MacDonald and F. C. Hawthorne, Canad. Mineral. **33**, 849 (1995).

34. G. Weber, E. Sciora, J. Guichard, F. Bouyer, I. Bezverkhyy, J. Marcos Salazar, C. Dirand, F. Bernard, H. Lecoq, and R. Besnard, J. Therm. Anal. Calorim. **132**, 1055 (2018).

35. M. R. Abass, W. M. El-Kenany, and E. H. El-Masry, Environ. Sci. Pollut. Res. **29**, 72929 (2022).

36. M. Gabr, K. A.-A. Ali, and A. G. E.-D. Mostafa, Turkish J. Phys. **31**, 31 (2007).

37. A. P. Reddy, P. N. Rao, M. Reddy, B. A. Rao, and N. Veeraiah, Appl. Phys. A **126**, 1 (2020).

38. J. H. Limón-Pacheco, N. Jiménez-Barrios, A. Déciga-Alcaraz, A. Martínez-Cuazitl, M. M. Mata-Miranda, G. J. Vázquez-Zapién, J. Pedraza-Chaverri, Y. I. Chirino, and M. Orozco-Ibarra, Toxics **8**, 51 (2020).

39. Z. A. Mekawy, E. A. A. El Shazly, and M. R. Mahmoud, J. Radioanal. Nucl. Chem. **331**, 4731 (2022).

40. M. R. Abass, A. B. Ibrahim, and M. M. Abou-Mesalam, Chem. Papers **75**, 3751 (2021).

41. M. R. Abass, E. H. El-Masry, and W. M. El-Kenany, J. Inorg. Organometal. Polym. Mater. **32**, 536 (2022).

42. A. Nilchi, B. Maalek, A. Khanchi, M. G. Maragheh, and A. Bagheri, Radiat. Phys. Chem. **75**, 301 (2006).

43. S. A. Nabi and A. M. Khan, React. Funct. Polym. **66**, 495 (2006).

44. M. A. Sayed, A. I. Helal, S. M. Abdelwahab, H. H. Mahmoud, and H. F. Aly, Chem. Papers **74**, 619 (2020).

45. G. Sheng, J. Hu, H. Jing, S. Yang, X. Ren, J. Li, Y. Chen, and X. Wang, Radiochim. Acta **98**, 291 (2010).

46. V. K. Gupta, S. Agarwal, I. Tyagi, D. Pathania, B. S. Rathore, and G. Sharma, Ionics **21**, 2069 (2015).

47. I. M. El-Naggar, E. S. Sheneshen, and E. A. Abdel-Galil, Partic. Sci. Technol. **34**, 373 (2016).

48. E. H. Borai, M. F. Attallah, A. H. Elgazzar, and A. S. El-Tabl, Partic. Sci. Technol. **37**, 414 (2019).

49. M. R. Abass, R. M. Maree, and N. M. Sami, Int. J. Environ. Anal. Chem. **104**, 103 (2024).

50. E. A. Abdel-Galil, A. B. Ibrahim, and M. M. Abou-Mesalam, Int. J. Ind. Chem. **7**, 231 (2016).

51. M. M. Abou-Mesalam, Colloids Surfaces A: Physicochem. Eng. Asp. **225**, 85 (2003).

52. I. M. El-Naggar, E. A. Mowafy, E. A. Abdel-Galil, and M. F. El-Shahat, Global J. Phys. Chem. **1**, 91 (2010).